

Multi-axial Failure Strengths of Open-Cell Foams with Tetrakaidecahedral Cells Using Finite Element Analysis

Prasanna Thiyyagasundaram,¹ Bhavani V. Sankar,² Nagaraj K. Arakere³

Department of Mechanical & Aerospace Engineering, University of Florida, Gainesville, Florida, 32611-6250

Finite element method based micromechanics has been used for predicting the multi-axial failure strengths of open cell foams which have tetrakaidecahedral unit-cells. Low density foams with equi-sided and Kelvin-elongated tetrakaidecahedron as unit cells are studied. The struts are modeled using three-dimensional beam elements. The effect of varying cross section on the failure strengths is presented. Failure envelopes for two-dimensional and three-dimensional stress states are plotted for foams with equisided and elongated tetrakaidecahedron unit cells. Effect of anisotropy in foams with elongated tetrakaidecahedral unit cells on the failure envelopes is also discussed.

I. Nomenclature

a_1	=	Length of the representative volume element
a_2	=	Width of the representative volume element
a_3	=	Height of the representative volume element
V	=	Volume of the representative volume element
f_{ij}	=	Force in the direction j when displacement is applied in the direction i
$\epsilon_1, \epsilon_2, \epsilon_3$	=	Strain components in the principal X, Y, Z directions
$[C]$	=	Stiffness matrix of the foam
u_i	=	Displacement in the i direction
ϵ_0	=	Applied macro-strain
E_i	=	Young's modulus in the i direction
G_{ij}	=	Shear modulus in direction j on the plane whose normal is in direction i
ν_{ij}	=	Poisson's ratio
I_x, I_y	=	Moment of inertia in the X and the Y directions
J	=	Torsion constant
ρ_s	=	Density of the strut material
E_s	=	Elastic modulus of the strut material
ν_s	=	Poisson ratio of the strut material
A	=	Cross sectional area of the strut
d	=	Length of the side of the equilateral triangle cross section
l	=	Length of each strut in the tetrakaidecahedron
r	=	Radius of the 3-cusp hypocycloid cross section
Δu_i	=	Difference in translational displacement along axis i
$\Delta \theta_i$	=	Difference in rotational displacement along axis i
b	=	Dimension of the top, bottom squares of the elongated tetrakaidecahedron unit cell
L	=	Dimension of the long edges of the elongated tetrakaidecahedron unit cell
S^*	=	Failure strength of the constituent strut material
S_i	=	Principal stress in the strut

¹Graduate Student & Corresponding Author, (pthiyaga@ufl.edu)

²Newton C. Ebaugh Professor, Associate Fellow AIAA. (sankar@ufl.edu)

³Associate Professor, (nagaraj@ufl.edu)

II. Introduction

Cellular polymeric foams are finding wide applications in energy absorption devices, insulators, packaging, and cores of sandwich panels. Cellular foams are lightweight, highly compressible and have useful mechanical, thermal and acoustic properties. Gibson and Ashby [1] define foams as special cellular materials constituting solid struts or thin plate like materials bridged together. Foams are generally made by dispersing gas into a liquid material and then cooling it to solidify. Foams in comparison to solid metals and ceramics have been found to have lower thermal conductivity, lower density and capacity to absorb large amount of energy.

Advanced foams have found a great potential for use in automotive, aircraft, and space vehicle structures. A special application of these materials is to provide thermal insulation to external fuel tanks and thermal protection systems (TPS) of space vehicles. Polyurethane foams have been the material of choice for external fuel tank insulation of space vehicles due to low density. With ongoing research focused on areas such as understanding mechanisms that cause foam fracture and debris liberation [2] during takeoff and during the operation of the space vehicle, a thorough understanding of this foam's mechanical response behavior, in the form of an accurate characterization of its strength and stiffness properties would be an essential step and is the main objective of the current work.

Foam cells result from a blowing-gas diffusing into bubbles that are nucleated or stirred into the system at the time of mixing. As early as 1887, Thompson [3] showed that packed in a BCC structure, a tetrakaidecahedron – a 14-faced polyhedron – is the shape that satisfies the minimum surface energy condition for mono-dispersed bubbles. Microcellular graphitic carbon foams were first developed at the US Air Force Research Laboratory in the 1990s [4]. Further, studies on foams [5] have confirmed that the repeating unit cell of foam resulting from a bubble nucleation process is a tetrakaidecahedron.

With this recognition of a repeating pattern, principles of micromechanics have been used [6] to characterize cellular foams. These methods are based on simulating a characteristic representative part of the structure that periodically repeats itself, instead of simulating the entire model. Foams with simple representative unit cell structures such as cube [7], to hexagonal cell structures, to a regular tetrakaidecahedron [8] as the unit cell, have been studied and have been characterized for their mechanical behavior.

The literature available on characterizing the mechanical response of foams can be broadly classified into analytical [9,10,11,12] and experimental [13,14,15].

Analytical models that have been developed focus primarily on predicting mechanical and strength properties. Assuming that the unit cell edges behave like a three dimensional beam, the mechanics of deformation of the tetrakaidecahedron unit cell leads to a set of equations for the effective Young's modulus, Poisson's ratio and tensile strength of the foam in the principal material directions [10,12]. The equations for these elastic constants have been derived and have been written in terms of the cell edge length, and the axial, flexural and torsional rigidities of the strut cross section. Also the variation of these properties with relative density (the ratio of the density of the cellular medium to the density of the solid strut material) of the foam has been expressed. Currently, BX-265 and NCFI24-124 are the two foams used to insulate the space shuttle external tanks. The photomicrographs of these two foams are shown in Figures 1a and 1b. Analysis of the foam structure from these micrographs has shown that due to forming and rising processes that takes place during fabrication, the unit cell of these foams is elongated in one of the three principal directions. Hence, this unit cell is called an elongated tetrakaidecahedron and the elongated direction is referred to as the rise direction. This makes the elongated foam orthotropic.

In a comprehensive study, Sullivan et al [15] in their experiments on BX265 and NCFI 24-124 come up with the trends for the stress-strain curves for obtaining material properties (Figure 2). As shown in the figure, the anisotropy of the foam structure is evident, as the stiffness in the rise direction is higher than the stiffness in the direction perpendicular to rise direction.

Sullivan et al also continue to derive analytical models for these foams with elongated tetrakaidecahedral unit cells. Their procedure is an extension of procedures used by Zhu et al [12] in deriving equations for foams with unit cells made out of equisided tetrakaidecahedron. They also derive equations for elastic moduli, poisson ratios and shear moduli. They also capture the variation of these properties with relative density.

In a previous study [20] the authors used a finite element based micromechanics procedure to calculate the stiffness properties of foam materials with both equisided and elongated unit cells. In this study the methods are extended to calculate multi-axial failure strengths.

Failure strengths have been calculated using direct micromechanics based methods [16, 17, 18, 21]. These methods use the method of superposition, in which a micro-stress field in the unit cell is determined for any given

homogenous macro-stress field applied on the foam. The failure criterion for the strut material is assumed to be known in this study. The foam is assumed to have failed if one of the struts in the unit cell fails due to the applied macro-stress field.

III. Stiffness properties using finite element based micromechanics methods

A general tetrakaidecahedron having 24 vertices, 36 edges made of 8 six-sided polygons and 6 four-sided polygons (Figure 3) is more precisely called truncated octahedron; since it is created by truncating the corners of an octahedron [19]. This is called an equi-sided tetrakaidecahedron. If it is generated by truncating the corners of a cuboid or hexahedron, it is called an elongated tetrakaidecahedron. Details about the geometry of the equi-sided and elongated tetrakaidecahedron are given in [20].

In this study, commercially available ABAQUS[®] finite element software is employed for developing the model. A finite element model for the equi-sided tetrakaidecahedron made out of beam elements for struts is shown in Figure 4. The principal directions X , Y , and Z are considered to be along the lines passing through the centers of the squares on the front and back, the left and right and the top and the bottom, respectively. It should be noted that out of the 36 edges in the geometry, only 24 beam elements have been modeled. This is due to periodicity of the unit cell. Elaborate details about the equisided and elongated tetrakaidecahedron finite element beam models have been explained elsewhere [20]. The geometry dimensions and the material properties of the constituent strut material used in the equi-sided tetrakaidecahedron model are listed in Table 1. The strut material is considered as isotropic. In the current example the beam cross sections are approximated to be an equilateral triangle. Similar to an equisided tetrakaidecahedron, the geometry and the material properties of the constituent strut material used in the elongated tetrakaidecahedron model are listed in Table 2. The strut material is again considered to be isotropic. Using beam elements in the model requires a slenderness ratio (L/r' , where L is the length of the strut, r' is the radius of gyration defined by $r'^2=I/A$) to be greater than about 10. If the slenderness ratio is less than 10 but greater than 6, one can use shear-deformable beam elements and hope to obtain good results. If L/r' is less than 6, one cannot use beam elements to model the deformation of the struts. One needs to resort to solid elements.

For both equi-sided and elongated tetrakaidecahedrons, two-node beam elements (classical Euler-Bernoulli beam element, B33 in the ABAQUS[®] material library) with cubic formulation were used to model the unit cell. Three-node quadratic elements (shear deformable Timoshenko beam elements, B32 in the ABAQUS[®] material library) were used in some cases to study the effects of shear deformation on the overall properties of the foam.

Boundary conditions to be applied on the finite element model are obtained by relating micro-strains to the corresponding macro-strains. From the periodicity of the cell structure, the representative volume element (RVE) is identified to be the smallest cuboid that completely encloses the tetrakaidecahedron such that 6 square sides of the tetrakaidecahedron are on the 6 faces of the cuboid. The periodic boundary conditions that are applied on the unit cell surfaces are summarized in Table 3 and the nodal pairs that are subjected to these PBCs are shown in Figures 5a to 5c.

Further to applying the above periodic boundary conditions on the model, the equivalent orthotropic material properties with its principal material directions parallel to the edges of the cuboid are calculated as follows. It should also be noted that in this coordinate system the normal and shear deformations are uncoupled. First we derive the equations to determine the Young's moduli and Poisson's ratios in the principal material coordinates, 1, 2 and 3. The (macro-scale) stress-strain relations of the foam are written as:

$$\begin{Bmatrix} \sigma_1 \\ \sigma_2 \\ \sigma_3 \end{Bmatrix} = \begin{bmatrix} C_{11} & C_{12} & C_{13} \\ C_{21} & C_{22} & C_{23} \\ C_{31} & C_{32} & C_{33} \end{bmatrix} \begin{Bmatrix} \varepsilon_1 \\ \varepsilon_2 \\ \varepsilon_3 \end{Bmatrix} \quad (1)$$

We subject the RVE to three independent deformations such that in each case only one normal strain is non-zero and other two normal strains are zero. For example, in the first case we apply periodic boundary conditions such that the cuboid expands only in the 1-direction and the strains in the other two directions are equal to zero, i.e., the dimensions of the cuboid in those directions do not change. Then the macro-strains are given by:

$$\varepsilon_1 = 1, \varepsilon_2 = 0 \text{ and } \varepsilon_3 = 0 \quad (2)$$

Substituting Eq. (10) in (9), we get

$$\begin{Bmatrix} \sigma_1 \\ \sigma_2 \\ \sigma_3 \end{Bmatrix} = \begin{bmatrix} C_{11} & C_{12} & C_{13} \\ C_{21} & C_{22} & C_{23} \\ C_{31} & C_{32} & C_{33} \end{bmatrix} \begin{Bmatrix} 1 \\ 0 \\ 0 \end{Bmatrix} \quad (3)$$

Let the corresponding force resultants (ABAQUS® output) in the three faces of the unit cell normal to the 1, 2 and 3 directions be, respectively, F_{11} , F_{21} and F_{31} (see Figure 6). Then the corresponding macro-stresses are obtained as:

$$\sigma_1 = \frac{F_{11}}{A_1}, \sigma_2 = \frac{F_{21}}{A_2}, \sigma_3 = \frac{F_{31}}{A_3} \quad (4)$$

where A_1 , A_2 and A_3 are areas normal to the 1, 2 and 3 directions which would be areas of the square surfaces in the 1, 2, 3 directions of the representative volume element in case of the equisided tetrakaidecahedron unit cell and the areas of the rectangular surfaces in the 1, 2, 3 directions of the representative volume element in case of the elongated tetrakaidecahedron unit cell.

Substituting for the macro stresses and strains in Eq. (1) we obtain

$$C_{11} = F_{11}, C_{21} = F_{21}, C_{31} = F_{31}, \quad (5)$$

Similarly we can deform the RVE in the other two directions and calculate second and third columns of $[C]$. For the case of shear, the calculations can be simplified, as there is no coupling between shear deformation and the normal deformation, and also between shear deformations in different planes. The straightforward method of determining the shear modulus G_{ij} will be to relate the strain energy in the RVE to the strain energy density due to shear:

$$U = \frac{1}{2} G_{ij} \gamma_{ij}^2 V \text{ or } G_{ij} = \frac{2U}{\gamma_{ij}^2 V} \quad (6)$$

The elastic constants of the foam with varying cross section could be determined by following the procedures similar to that of uniform cross section foam. In fact the struts can be modeled using one beam element as before but with equivalent cross sectional properties. Since the deformations (strains, curvatures, etc.) in a beam are inversely proportional to A, I, J it is obvious that the equivalent uniform cross sectional properties could be obtained as

$$\frac{1}{A_{eff}} = \frac{1}{l} \int_{-l/2}^{l/2} \frac{dx}{A(x)},$$

$$\frac{1}{I_{eff}} = \frac{1}{l} \int_{-l/2}^{l/2} \frac{dx}{I(x)}, \quad (7)$$

$$\frac{1}{J_{eff}} = \frac{1}{l} \int_{-l/2}^{l/2} \frac{dx}{J(x)}$$

Where the suffix *eff* denotes effective properties. In order to determine the above effective properties, one has to assume the nature of the cross section. In this study we assume the cross section of the strut is an equilateral triangle. Then the cross sectional dimension at the midspan d_0 , corresponding area A_0 and the moments of inertia I_0 and J_0 are calculated as follows:

$$A_0 = \frac{\sqrt{3}}{4} d_0^2 \quad (8)$$

$$I_0 = \frac{\sqrt{3}}{96} d_0^4 \quad (9)$$

$$J_0 = \frac{A_0^2}{5\sqrt{3}} \quad (10)$$

Then the variation of moments of inertia using equation along the length of the strut can be written as

$$I(x) = I_0 \left[86 \frac{x^4}{l^4} + \frac{x^2}{l^2} + 1 \right]^2, \quad (11)$$

$$J(x) = J_0 \left[86 \frac{x^4}{l^4} + \frac{x^2}{l^2} + 1 \right]^2$$

$$\text{where, } -\frac{l}{2} \leq x \leq +\frac{l}{2}$$

It is desirable to compare the properties of foam with struts having a varying cross-section to foam with struts having uniform cross-section. One approach to get a good comparison is by keeping the relative density same in both the cases. This can be achieved by keeping the volume of the strut same in both cases:

$$\int_{-l/2}^{+l/2} A(x) dx = \bar{A} l \quad (12)$$

where, \bar{A} is the area of the uniform cross-section, l is the length of the strut. Once \bar{A} is calculated, one can determine the corresponding cross section dimension \bar{d} , and the moments of inertia \bar{I} and \bar{J} .

IV. Direct Micromechanics Method (DMM) to compute multi-axial failure strengths

Analytical models have been formulated for both stiffness properties and failure strengths by Zhu et al [12] and Sullivan et al [15] where they assume that the failure strength of the foam occurs when the constituent element strut undergoes brittle failure. However, in these analytical models, the formulations are limited to cases of the foam structure experiencing a uniaxial state of stress. However, in reality, foam structures experience multi-axial states of stress. Direct Micromechanics Methods (DMM) deals with this limitation very effectively.

The DMM was originally proposed by Sankar et al. and has been demonstrated in several of his works [16,17,18]. In Zhu et al. [21] the failure envelopes obtained from DMM are compared with the phenomenological failure criteria for plane stress states and they have been shown to match well. A similar observation, based on experimental results, has made by Daniel and Ishai [22], where again it is recommended that one should use several failure criteria and choose the most conservative criterion for a given state of stress which seems to closely match the failure envelope that has been traced by DMM.

DMM can be considered as a computational laboratory to estimate failure strengths, the advantage being that a variety of loading conditions which may be hard to achieve through physical experiments can be simulated. For example, it is difficult to design a fixture and apply multi-axial loading beyond two or three dimensions. However, even a 6-dimensional state of load can be applied using DMM as it is a computational method.

The broader objective of predicting the failure strength of foam is computing a load factor for the foam when it is subjected to generalize given state of loading. The load factor is also equal to the factor of safety for the given set of stresses. The procedure that is adopted to calculate the load factor is as follows.

Consider a state of macro-stresses given by , $\{\sigma\} = \{\sigma_x \quad \sigma_y \quad \sigma_z \quad \tau_{xy} \quad \tau_{yz} \quad \tau_{xz}\}^T$. The macro-strains due to the above stresses can be calculated as:

$$\{\varepsilon\} = [C]^{-1} \{\sigma\} \quad (13)$$

where, $[C]$ is the stiffness matrix of the foam.

The above macro-strain $\{\varepsilon\}$ can be represented as, $\{\varepsilon\} = \{\varepsilon_{xx} \quad \varepsilon_{yy} \quad \varepsilon_{zz} \quad \gamma_{xy} \quad \gamma_{yz} \quad \gamma_{xz}\}^T$

This macro-strain manifests as micro-stresses in each constituent strut of the unit cell. We apply periodic boundary conditions on the unit cell surfaces corresponding to the above macro strains. Then the detailed stress field in all the 36 struts is calculated. These stresses are the micro-stresses corresponding to the applied macro-stress state. As mentioned earlier we assume that the failure criterion for the strut material is known. For example, if the strut fails in a brittle manner, one can use the maximum principal stress criterion.

Although the six macro-strains can to be applied to the unit cell simultaneously, in practice we use the principle of superposition. The micro-stresses in the struts are calculated for unit values each of the six macro-strain components. Then using the principle of superposition the stresses in the strut are calculated for a given macro-strain state.

From the above state of stress, principal stresses at that critical point can be calculated. Once the principal stresses are calculated, any appropriate failure theory can be used for calculating load factor For example, if the maximum stress theory is used for calculating the load factor, then the load factor is calculated as:

$$\lambda = \frac{S_*}{\max(|S_1|, |S_2|, |S_3|)} \quad (14)$$

where, S_* is the strength of the solid strut material, S_1, S_2, S_3 are the 3 principal stresses.

Thus load factor can be calculated for all the 36 struts and the lowest load factor would be the critical load factor for the given state of loading. If that lowest load factor is λ_L , then $\lambda_L \times \{\sigma\}$ would be the critical load that can be applied before the failure onset in the foam.

Thus, assuming a uniaxial state of external loading, the failure strength in the direction of application of the external load can be calculated using the same procedure as described above. Similarly, a biaxial state of external load or triaxial or a multiaxial state of external load can be applied and the load factor can be calculated.

V. Results and discussion – Stiffness Properties

The stiffness properties for both equisided and elongated tetrakaidecahedron unit cells are shown in Table 3 and Table 4, respectively. It is shown that the results for E and ν match well with the available analytical models – Model by Zhu, Knott, Mills [12] for equi-sided tetrakaidecahedron unit cell and the model by Sullivan, Ghosn, Lerch [15] for the elongated tetrakaidecahedron unit cell. The maximum error in the elastic constants was about 0.55% for the elastic moduli and 0.35% for the shear moduli in case of the equisided tetrakaidecahedron unit cell. The maximum error in the elastic constants was about 0.82% in the case of the elongated tetrakaidecahedron unit cell.

The results contrasting the values of elastic constants for the variable cross section foam with that of an idealized uniform cross section foam are presented in Table 5. The relative density is assumed to be 0.165% in both cases. It is seen that the Young's modulus and shear modulus of ideal foams with uniform cross section is about 2.4 times that of varying cross section foam. The reason for this is that most of the solid material being near the ends of the strut, thus making majority of length (about 60%) in the middle slender. This reduces the moments of inertia considerably making the struts more flexible.

Failure Strength results

Figure 7 shows the failure envelope for foam with equisided tetrakaidecahedral unit cells with constant strut cross section subjected to different states of biaxial stresses. It should be noted that it is purely coincidental that the failure envelope obtained resembles the Tresca (Maximum shear stress) failure theory. One interesting aspect of this result is that we assume the struts fail in a brittle manner. However, the failure of the foam at macro-scale mimics that of a ductile material. One should note that there are 36 struts in the unit cell. The six sides of the hexagon in Fig (7) indicate that the failure mode switches from one strut to another strut as the state of stress changes continuously. In general the failure envelope should be a 32-sided polygon, however due to material symmetry; there are only six sides to the failure envelope. This is shown in Figure 8. Figure 9 shows failure envelopes obtained for foam with equisided tetrakaidecahedral unit cells with constant strut cross section subjected to different states of biaxial stresses and an in-plane shear stress. This type of a loading is common in case of foams in the form of thin plates. As would be expected, as the magnitude of the in-plane shear stress is increased, the failure envelope shrinks to a point at the centre. Failure envelopes obtained for foam with equisided tetrakaidecahedral unit cells with constant strut cross section subjected to triaxial stresses has been shown in Figure 10. It should be noted that the stresses here have been plotted on a new coordinate axis such that it has a vector that is equally inclined to the old coordinate axis as one of its principal axes. This vector is called the hydrostatic vector and has direction cosines $\left(\frac{1}{\sqrt{3}}, \frac{1}{\sqrt{3}}, \frac{1}{\sqrt{3}}\right)$ in the $\sigma_1, \sigma_2, \sigma_3$ space. In Figure 10, S_1, S_2, S_3 along the coordinate axes represent this new coordinate system. As seen in Figure 10, the failure envelopes corresponding to each S_i are obtained to be hexagons and as this S_i is increased, the hexagons contract and approach to a point. This has been pictorially depicted in Figure 11. Figure 12 shows the contrast in the failure envelopes for foam with equisided tetrakaidecahedral unit cells with constant strut cross section and varying cross section subjected to different states of biaxial stresses. As would be expected, the failure strength with varying cross section is reduced to a third of the strength seen in the case of constant cross section.

Figure 13 shows the failure envelope for foam with elongated tetrakaidecahedral unit cells with constant strut cross section subjected to different states of biaxial stresses one applied in the rise-direction and the other applied in the perpendicular to rise-direction. In this case the failure envelope obtained does not look the same as that of the foam with equisided tetrakaidecahedral unit cells. The failure strength of the strut is assumed to be 0.17 GPa and the failure strength of the foam is obtained to be 1.7 MPa in the rise direction and 0.08 MPa in the perpendicular to rise directions. Failure envelope for foam with elongated tetrakaidecahedral unit cells with constant strut cross section subjected to different states of biaxial stresses applied on each of the perpendicular to rise-directions has been shown in Figure 14. In this case the failure envelope obtained looks the same in both the axes. For the failure strength of the strut assumed to be 0.17 GPa the failure strength obtained in the both the perpendicular to rise directions is 0.08 MPa. Figure 15 shows failure envelopes obtained for foam with elongated tetrakaidecahedral unit cells with constant strut cross section subjected to different states of biaxial stresses in the rise direction and the perpendicular-to-rise direction and an in-plane shear stress. As the magnitude of the in-plane shear stress is increased, the failure envelope shrinks to a point at the centre. Figure 16 shows failure envelopes obtained for foam with elongated tetrakaidecahedral unit cells with constant strut cross section subjected to different states of biaxial stresses both the perpendicular-to-rise directions and an in-plane shear stress. Again, as the magnitude of the in-plane shear stress is increased, the failure envelope shrinks towards the centre. Figure 17 shows failure envelopes obtained for foam with elongated tetrakaidecahedral unit cells with constant strut cross section subjected to triaxial stresses. Again as in the case of the equisided tetrakaidecahedral unit cell case, the envelopes are plotted in the hydrostatic plane. However, unlike that the equisided foam, the hexagons don't contract towards the centre. This is due to the anisotropic nature of the foam and warrants further investigation.

VI. Summary

A finite element based micromechanics has been used to calculate the elastic properties of foams with tetrakaidecahedral unit cells. It has been shown that the results for elastic constants match well with the available analytical models. A methodology to deal with varying cross sections has also been considered. The same finite element based micromechanics methods has been extended to generate multi-axial failure envelopes for foams with

both equisided and elongated tetrakaidecahedral unit cells. Again, the effect of varying cross-section on the failure envelope has been studied.

VII. References

- [1] Gibson, L. J., and Ashby, M. F., 1997. *Cellular Solids: structure and properties*. 1st edition, Cambridge university press, U.K.,
- [2] Arakere, N.K., Knudsen, E., Wells, D., McGill, P., Swanson, G., 2008 “Determination of mixed-mode stress intensity factors, fracture toughness, and crack turning angle for anisotropic foam material”, *International Journal of Solids and Structures*, 45, pp. 4936-4951.
- [3] Thomson, W., 1887. “On the division of space with minimum partitional area.” *Philosophical Magazine* Vol. 24, No. 151, p. 503.
- [4] Hall, R. B., and Hager, J. W., 1996. “Performance limits for stiffness-critical graphitic foam structures, Comparisons with high-modulus foams, refractory alloys and graphite-epoxy composites”. *Journal of Composite Materials* Vol. 30, No. 17, 1922-1937.
- [5] Wright L.S. and Lerch B.A., 2005, “Characterization of space shuttle insulative materials”, *NASA/TM-2005-213596*
- [6] Sankar, B.V., Marrey, R.V., 1997. “Analytical Method for Micromechanics of Textile Composites”, *Composites Science and Technology* 57: 703 – 713.
- [7] Choi, S., Sankar, B.V., 2005, “A micromechanical method to predict the fracture toughness of cellular materials”, *International Journal of Solids and Structures* 42: 1797-1817.
- [8] Jang, W.Y., Kraynik, A.M., Kyriakides, S., 2008, “On the microstructure of open-cell foams and its effect on elastic properties”, *International Journal of Solids and Structures*, Vol 45 pp.1845–1875
- [9] Li, K., Gao, X. L., and Roy, A. K., 2003. “Micromechanics model for three-dimensional open-cell foams using a tetrakaidecahedral unit cell and Castigliano's second theorem”, *Composites Science and Technology* 2003, vol. 63, pp. 1769-1781.
- [10] Sullivan, R.M., Ghosn, L.J., Lerch, B.J, 2008, “A general tetrakaidecahedron model for open-celled foams”, *International Journal of Solids and Structures* 45: 1754-1765
- [11] Sihna, S., Roy, A.K., 2004, “Modeling and prediction of bulk properties of open-cell carbon foam”, *Journal of the Mechanics and Physics of Solids* Vol 52 pp.167 – 191
- [12] Zhu, H.X., Knott, J.F., Mills, N.J., 1997, “Analysis of the Elastic Properties of Open-Cell Foams with Tetrakaidecahedral Cells”, *Journal of Mechanics and Physics of Solids*, Vol.45, No.3, pp. 319-343
- [13] Gong, L., Kyriakides, S., Jang, W.Y., 2005 “Compressive response of open-cell foams. Part I: Morphology and elastic properties”, *International Journal of Solids and Structures*, Vol 42 pp.1355–1379
- [14] Jang, W.Y., Kraynik, A.M., Kyriakides, S., 2008, “On the microstructure of open-cell foams and its effect on elastic properties”, *International Journal of Solids and Structures*, Vol 45 pp.1845–1875
- [15] Sullivan, R.M., Ghosn, L.J., Lerch, B.J, 2008, “Application of an Elongated Kelvin Model to Space Shuttle Foams”, *Journal of Spacecraft and Rockets* Vol. 46, No. 2.
- [16] Leong, M., B.V. Sankar, 2008, “Effect of Thermal Stresses on the Failure Criteria of Fiber Composites”, *Mechanics of Advanced Materials & Structures* (in press)
- [17] Rao, M.P., B.V. Sankar, G.Subhash, 2009, “Effect of Z-Yarns on the Stiffness and Strength of Three-Dimensional Woven Composites”, *Composites Part B* 40 (2009) 540-551
- [18] Stamblewski, C., B.V. Sankar, D.Zenkert, 2008, “Analysis of Three-Dimensional Quadratic Failure Criteria for Thick Composites using the Direct Micromechanics Method”, *Journal of Composite Materials* 42(7) 635-654
- [19] Weisstein, E. W., “Truncated Octahedron, MathWorld--A Wolfram Web Resource”:
<http://mathworld.wolfram.com/TruncatedOctahedron.html>
- [20] Thiyagasundaram, P., B.V. Sankar, N.K.Arakere, 2009, “Elastic Properties of Open-Cell Foams with Tetrakaidecahedral Cells Using Finite Element Analysis”, *AIAA Journal* (in press)
- [21] Zhu, H., B.V. Sankar, Marrey, R.V., 1998, “Evaluation of Failure Criteria for Fiber Composites Using Finite Element Micromechanics”, *Journal of Composite Materials* 32(8): 766-782
- [22] Daniel, I.M., Ishai, O., 1994, “Engineering Mechanics of Composite Materials”, Oxford University Press, New York, USA.
- [23] Sullivan, R.M., Ghosn, L.J., Lerch, B.J, 2009, “Shear moduli for non-isotropic, open-cell foams using a general elongated Kelvin foam model”, *International Journal of Engineering Science*, Vol 47 pp 990-1001

VIII.Figures

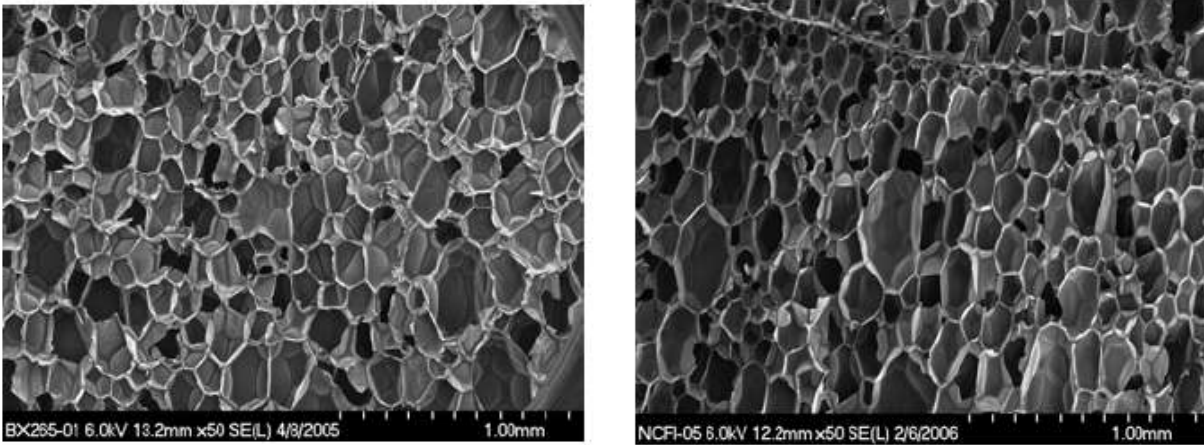


Figure 1. Photomicrographs of foams used in insulation of external fuel tanks of space vehicles a) BX-265 and b) NCFI24-124 (Ref. [10])

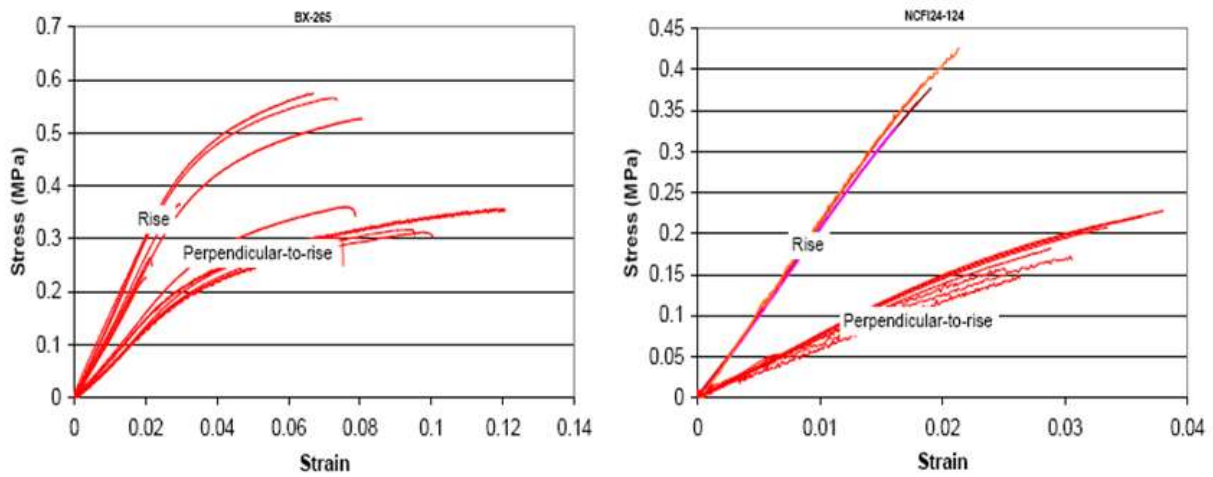


Figure 2. Stress-strain response for polyurethane foams used in external fuel tanks (Ref. [15])

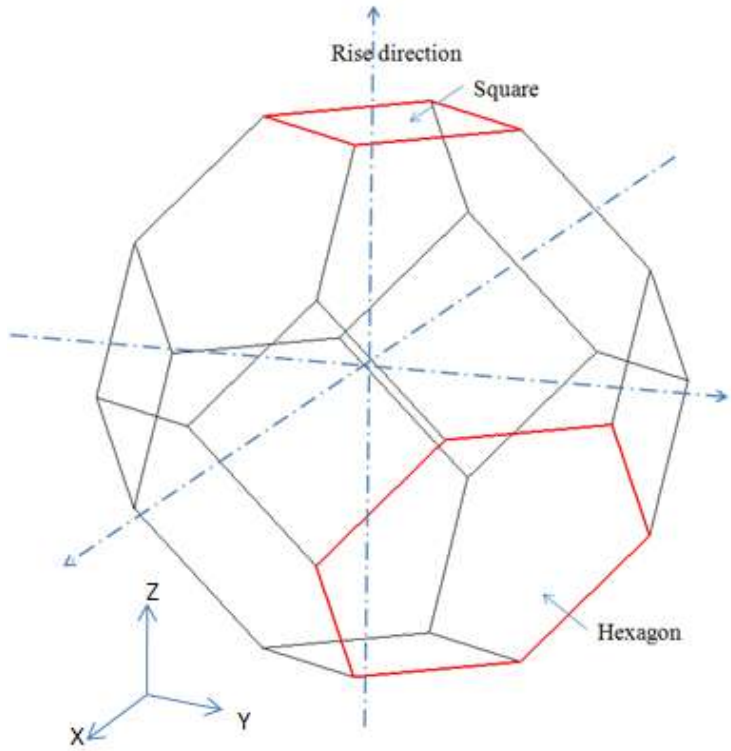


Figure 3. Equisided tetrakaidecahedron

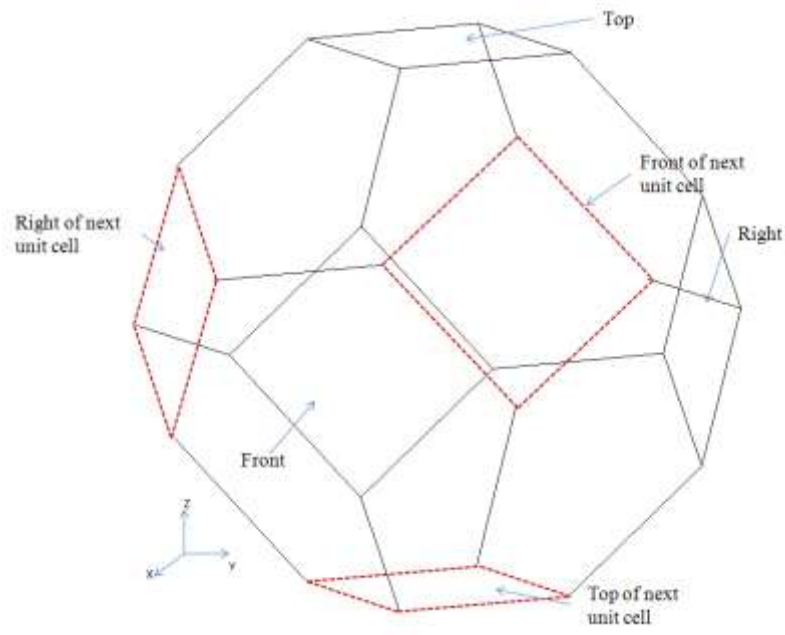


Figure 4. Equisided tetrakaidecahedron - Beam model with 24 struts

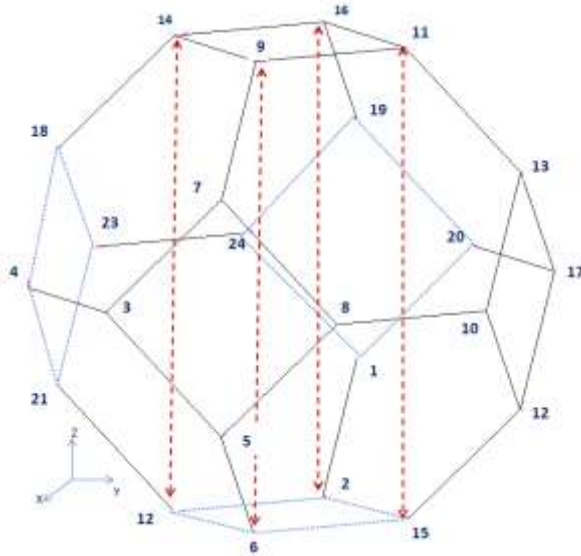


Fig 5a. Top & Bottom

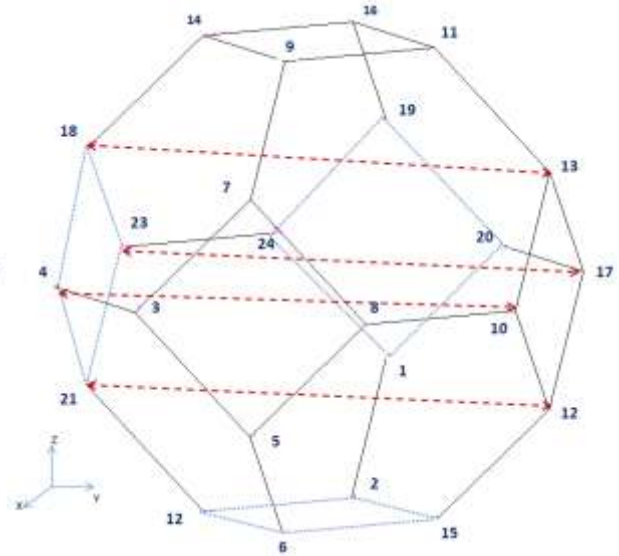


Fig 5b. Right & Left

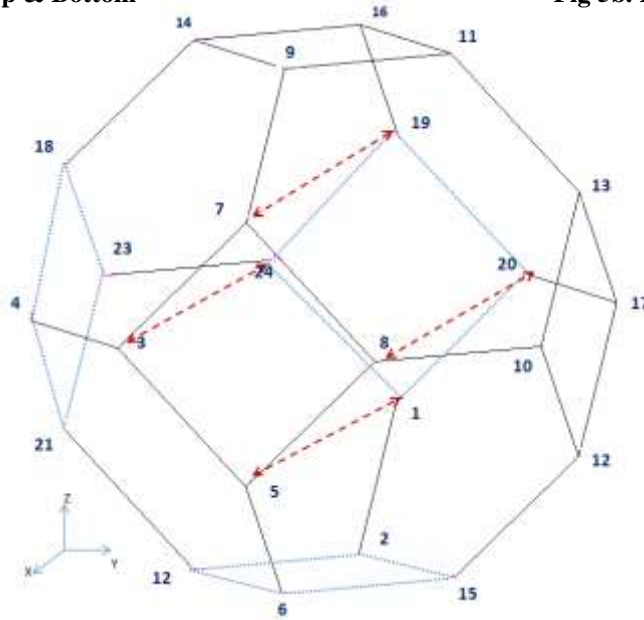


Fig 5c. Front & Back

Figure 5. Nodal Pairs subjected to Periodic Boundary Conditions (PBCs)

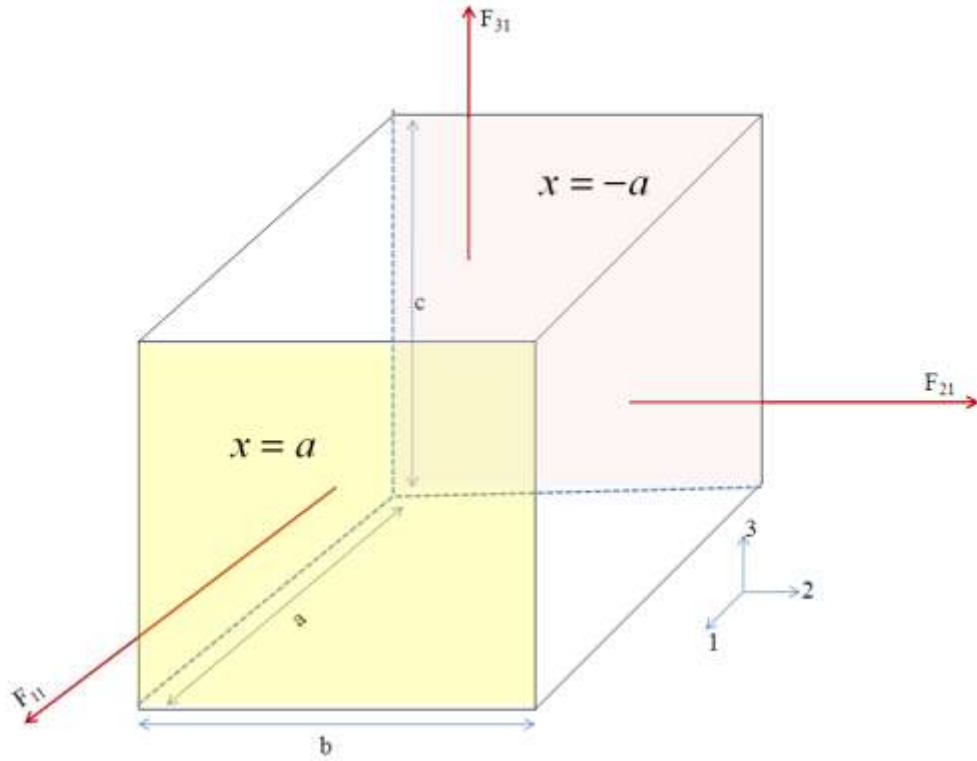


Figure 6. Representative Volume Element (RVE) showing force resultants in the 3 directions when subjected to normal strain in the 1-direction on the 2 faces $x = a, x = -a$

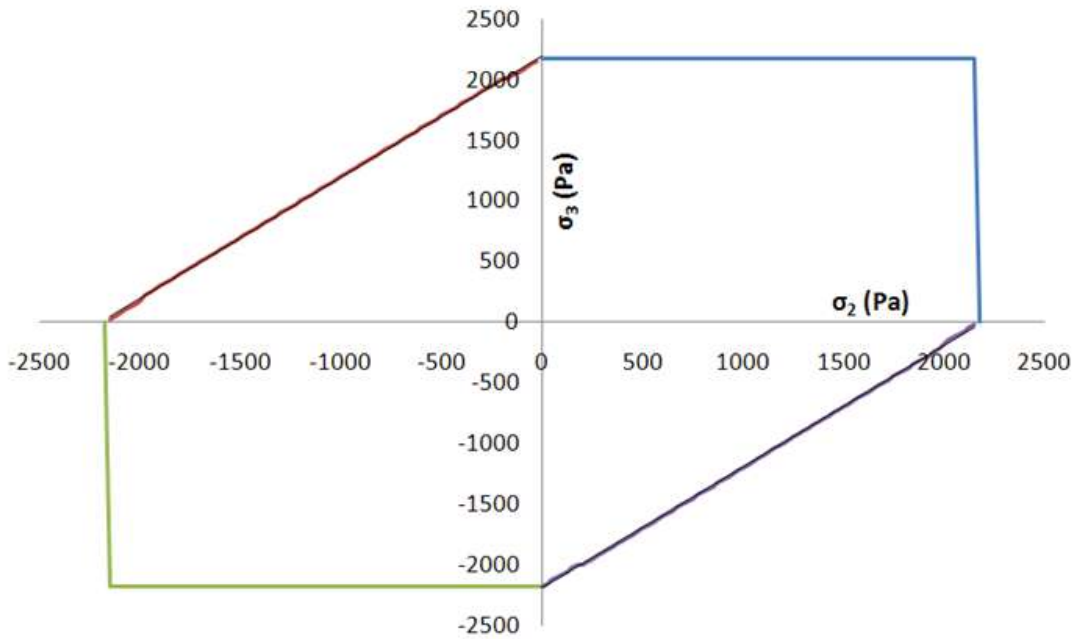


Figure 7. Failure envelope obtained from Direct Micromechanics Method (DMM) for an equisided tetrakaidecahedron (Table 1) with constant strut cross section subjected to a biaxial state of stress

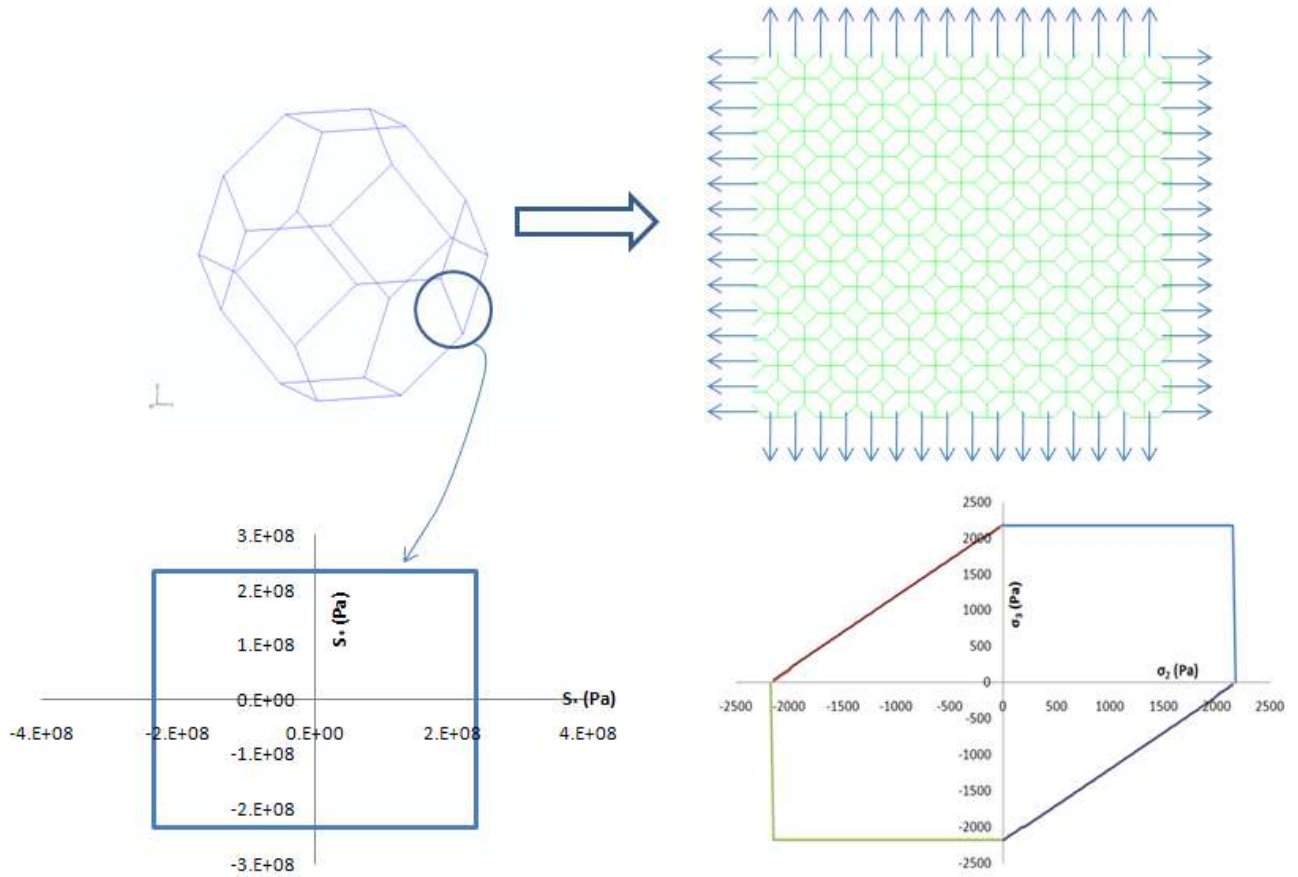


Figure 8. Maximum Normal stress failure (shown in the left) in the strut level manifests into the failure envelope as shown in the right for an equisided tetrakaidecahedron (Table 1) with constant strut cross section subjected to a biaxial state of stress

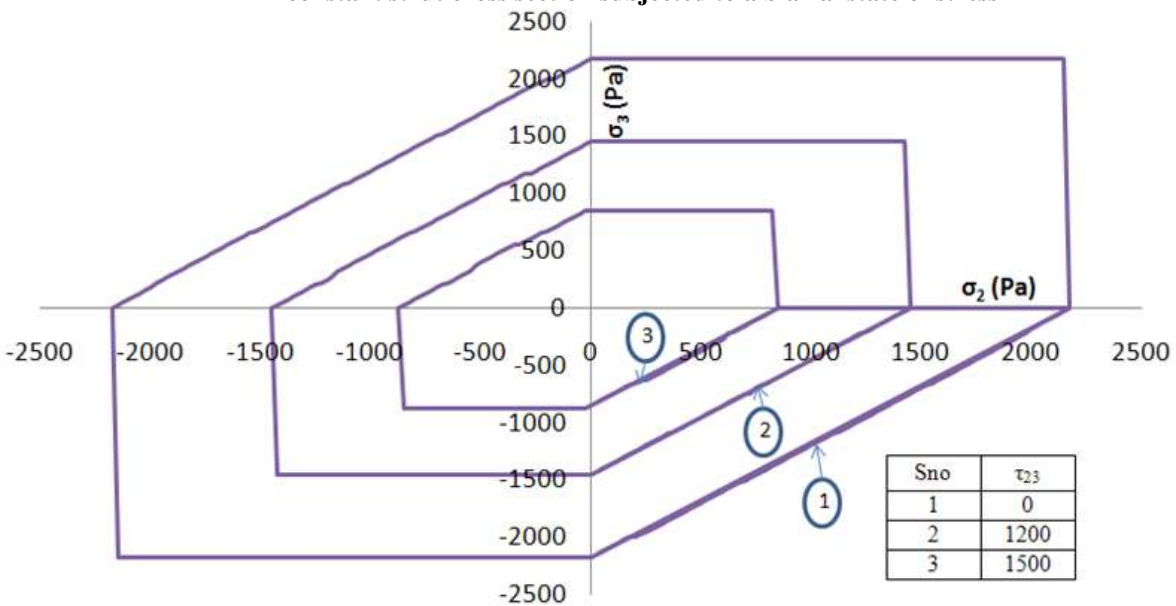


Figure 9. Failure envelope obtained from Direct Micromechanics Method (DMM) for an equisided tetrakaidecahedron (Table 1) with constant strut cross section subjected to a biaxial state of stress & an inplane shear stress

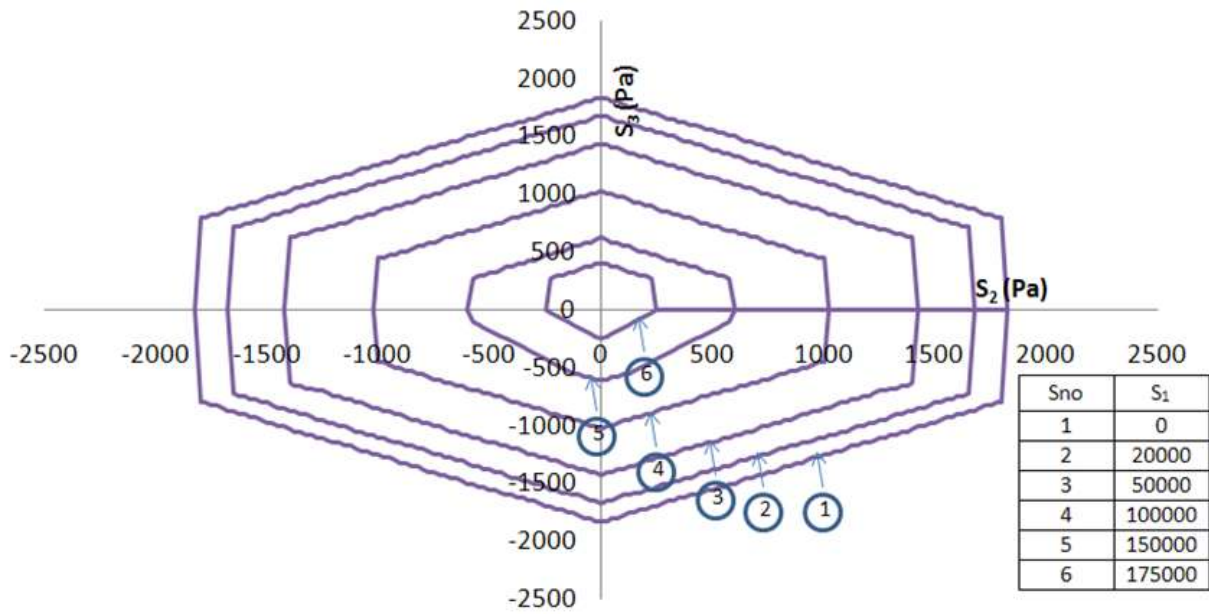


Figure 10. Failure envelope obtained from Direct Micromechanics Method (DMM) for an equisided tetrakaidecahedron (Table 1) with constant strut cross section subjected to a triaxial state of stress plotted on the hydrostatic plane

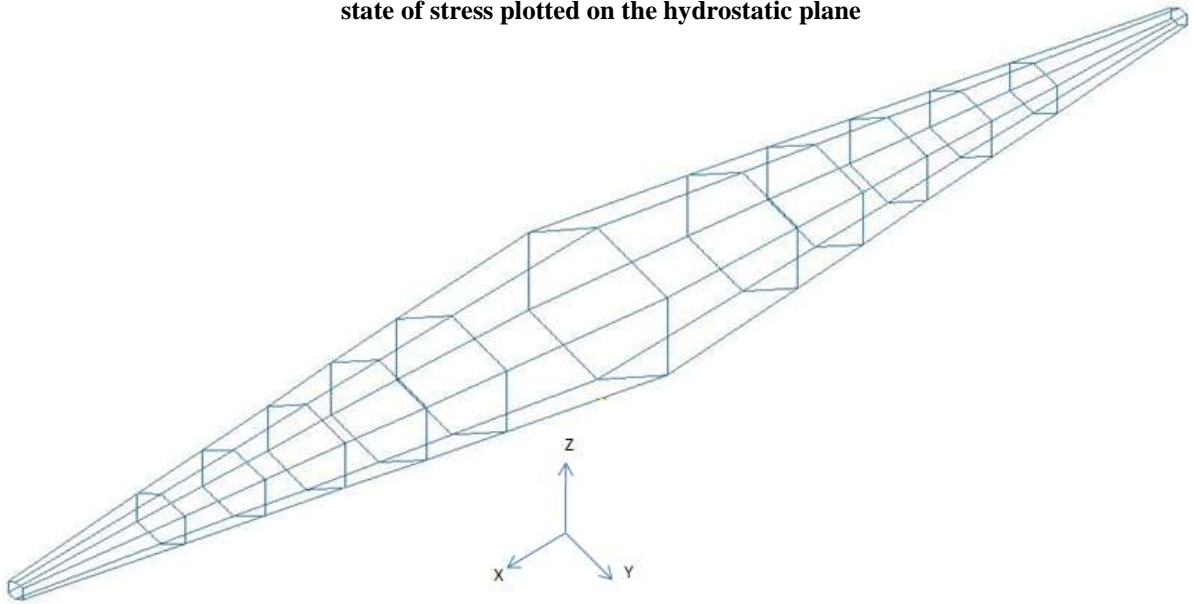


Figure 11. Pictorial (not to scale) representation of the Failure envelope obtained from Direct Micromechanics Method (DMM) for an equisided tetrakaidecahedron (Table 1) with constant strut cross section subjected to a triaxial state of stress plotted on the hydrostatic plane

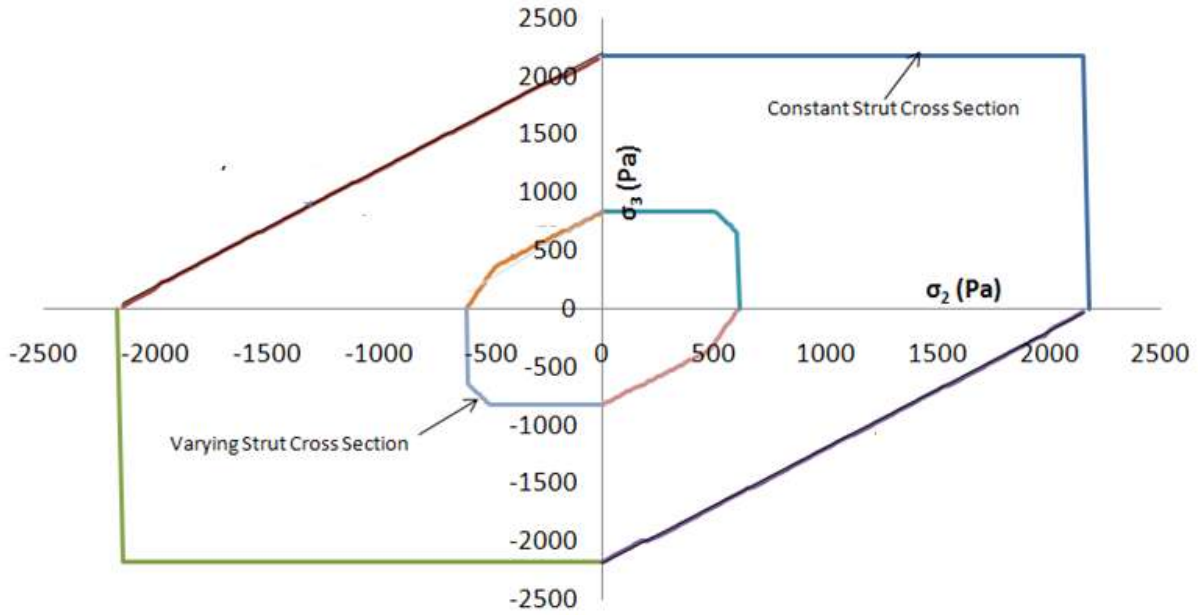


Figure 12. Failure envelopes obtained from Direct Micromechanics Method (DMM) for an equisided tetrakaidecahedron (Table 1) with constant and varying strut cross section subjected to a biaxial state of stress

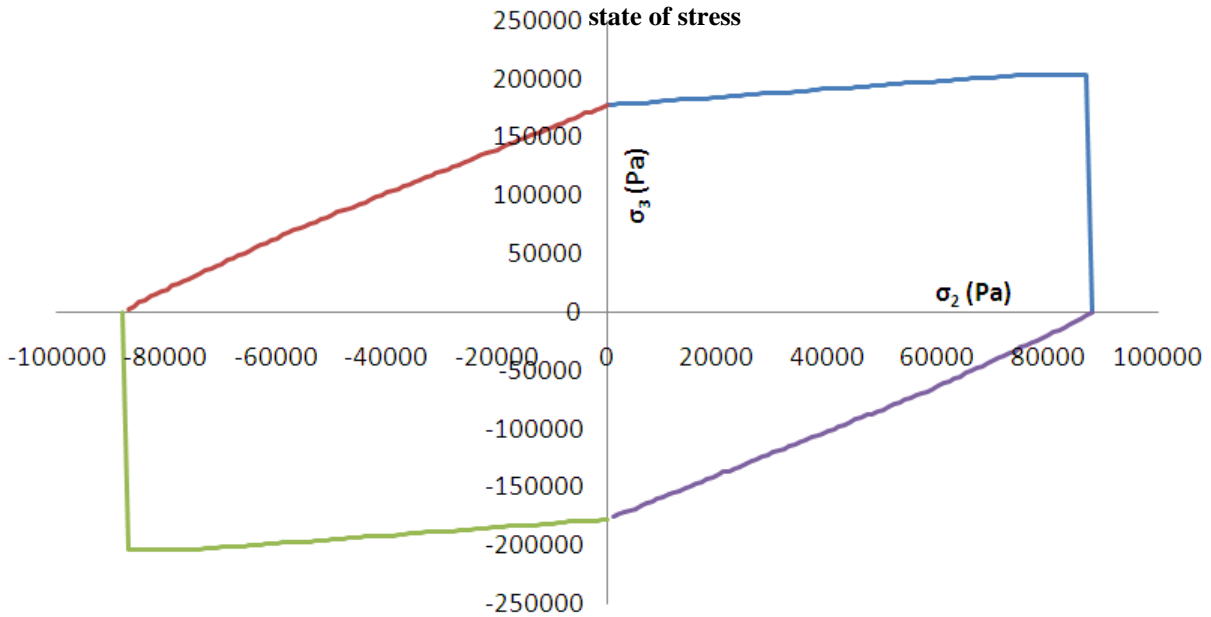


Figure 13. Failure envelope obtained from Direct Micromechanics Method (DMM) for an elongated tetrakaidecahedron (Table 2) with constant strut cross section subjected to a biaxial state of stress applied in the rise direction and the perpendicular-to-rise direction

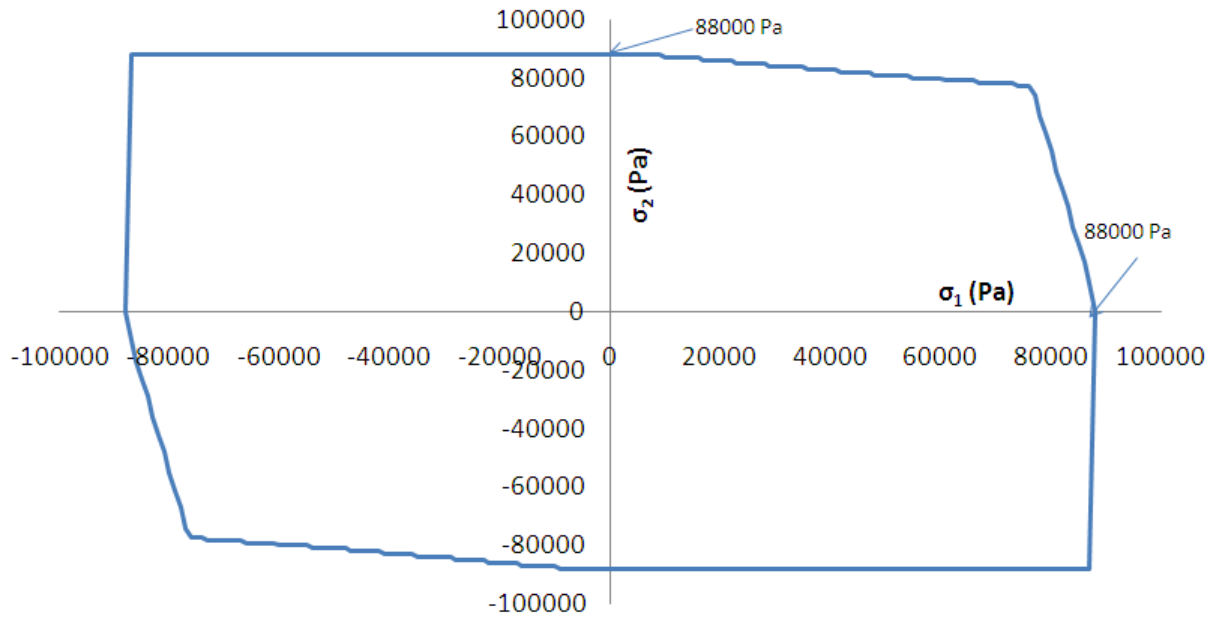


Figure 14. Failure envelope obtained from Direct Micromechanics Method (DMM) for an elongated tetrakaidecahedron (Table 2) with constant strut cross section subjected to a biaxial state of stress applied in both the perpendicular-to-rise directions

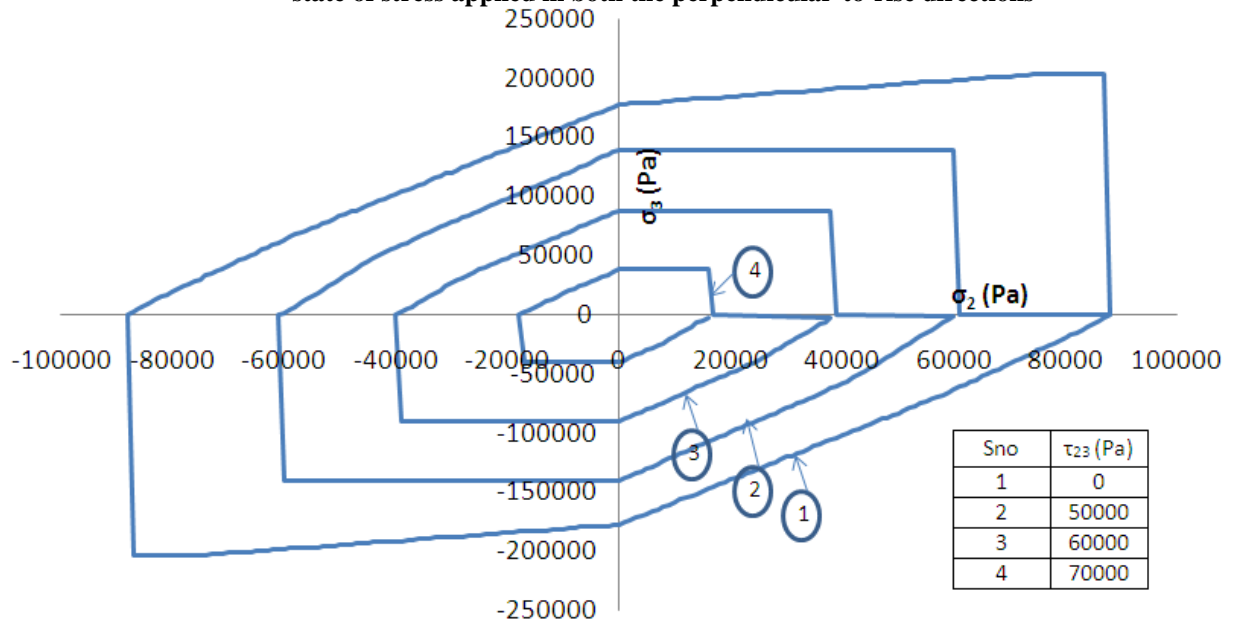


Figure 15. Failure envelope obtained from Direct Micromechanics Method (DMM) for an elongated tetrakaidecahedron (Table 2) with constant strut cross section subjected to a biaxial state of stress in the rise direction, perpendicular-to-rise & an inplane shear stress

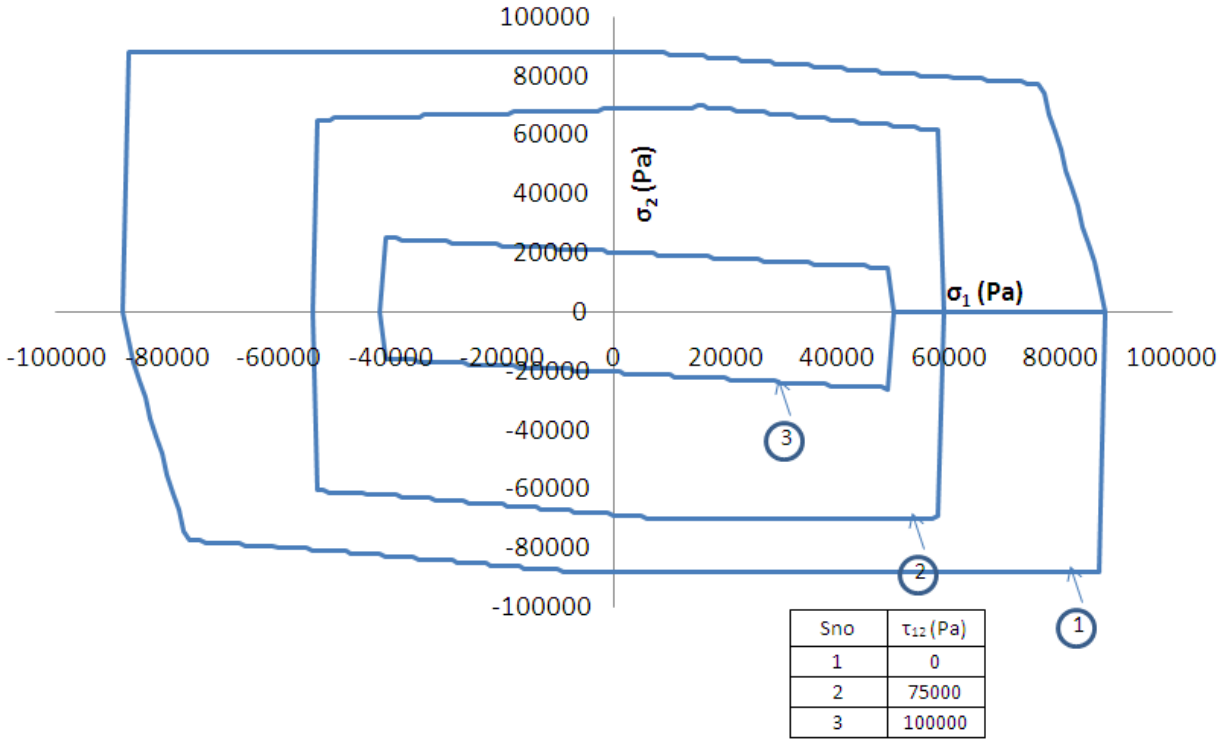


Figure 16. Failure envelope obtained from Direct Micromechanics Method (DMM) for an elongated tetrakaidecahedron (Table 2) with constant strut cross section subjected to a biaxial state of stress both the perpendicular-to-rise directions & an inplane shear stress

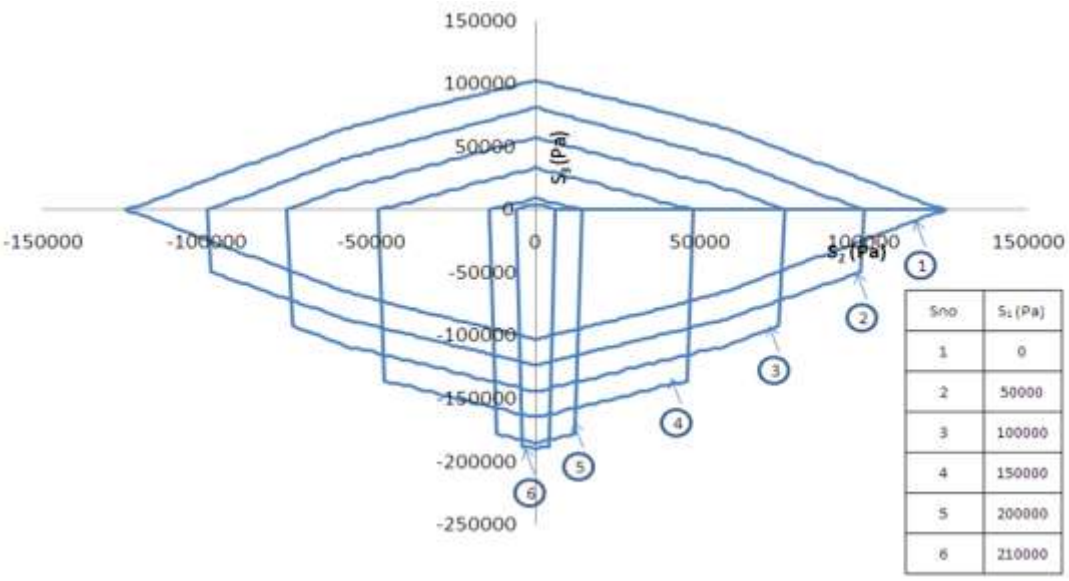


Figure 17. Failure envelope obtained from Direct Micromechanics Method (DMM) for an elongated tetrakaidecahedron (Table 2) with constant strut cross section subjected to a triaxial state of stress plotted in the hydrostatic plane

IX. Tables

Table 1: Material properties of the strut, geometric properties, cross Sectional properties of the equisided tetrakaidecahedron unit cell

Material Properties of the strut	Density, ρ_s (Kg/m ³)	1650
	Elastic modulus, E_s (GPa)	23.42
	Poisson ratio, ν_s	0.33
	Ultimate Tensile Strength, S_* (GPa)	0.2342
Geometry of the equisided tetrakaidecahedron unit cell (Fig. 3)	L (mm)	1
	d (mm)	0.06
	Relative density	0.001653
Cross-section properties (Equilateral Triangle)	Cross sectional area, A (m ²)	1.5588×10^{-9}
	Moment of Inertia, I_x, I_y (m ⁴)	2.3382×10^{-19}
	Torsion constant, J (m ⁴)	4.6765×10^{-19}

Table 2: Material properties of the strut, geometric properties, cross Sectional properties of the elongated tetrakaidecahedron unit cell

Material Properties of the strut	Density, ρ_s (Kg/m ³)	1650
	Elastic modulus, E_s (GPa)	17
	Poisson ratio, ν_s	0.33
	Ultimate Tensile Strength, S_* (GPa)	0.17
Geometry of the elongated tetrakaidecahedron unit cell (Fig. 5)	L (μ m)	77.2
	b (μ m)	35.6
	θ (degrees)	53.57
	r (μ m)	26
	H (μ m)	248.85
	D (μ m)	142.04
	Relative density	0.03481
Cross-section properties (3-cusp hypocycloid)	Cross sectional area, A (m ²)	1.024×10^{-10}
	Moment of Inertia, I_x, I_y (m ⁴)	1.403×10^{-21}
	Torsion constant, J (m ⁴)	2.806×10^{-21}

Table 3: Periodic Boundary conditions

Macrostrain		Non-Zero Displacement BC's
1	$\varepsilon_1 = 1$	$u_1(a_1, x_2, x_3) - u_1(0, x_2, x_3) = a_1$
2	$\varepsilon_2 = 1$	$u_2(x_1, a_2, x_3) - u_2(x_1, 0, x_3) = a_2$
3	$\varepsilon_3 = 1$	$u_3(x_1, x_2, a_3) - u_3(x_1, x_2, 0) = a_3$
4	$\gamma_{23} = 1$	$u_2(x_1, x_2, a_3) - u_2(x_1, x_2, 0) = a_3/2$
		$u_3(x_1, a_2, x_3) - u_3(x_1, 0, x_3) = a_2/2$
5	$\gamma_{31} = 1$	$u_1(x_1, x_2, a_3) - u_1(x_1, x_2, 0) = a_3/2$
		$u_3(a_1, x_2, x_3) - u_3(0, x_2, x_3) = a_1/2$
6	$\gamma_{12} = 1$	$u_1(x_1, a_2, x_3) - u_1(x_1, 0, x_3) = a_2/2$
		$u_2(a_1, x_2, x_3) - u_2(0, x_2, x_3) = a_1/2$

Table 4: Results obtained for the properties of Equisided Tetraikadecahedron Unit cell with relative density 0.1653%

Property	Finite Element Model			Analytical Model (Ref. [14])	% difference between analytical and Finite Element Model
	Euler-Bernoulli (2-node cubic)	Shear deformable (3- node quadratic)	% difference between Euler- Bernoulli model and Shear-deformable model		
$E_x = E_y = E_z$ (GPa)	46.7×10^{-6}	46.6×10^{-6}	0.24	46.4×10^{-6}	0.55
$\nu_{xy} = \nu_{yz} = \nu_{xz}$	0.498	0.498	0.11	0.497	0.14
$G_{xy} = G_{yz} = G_{xz}$ (GPa)	14.9×10^{-6}	14.8×10^{-6}	0.43	14.9×10^{-6}	0.35

Table 5: Results obtained for the properties of Elongated Tetraikadecahedron Unit cell with relative density 3.45%

Property	Finite Element Model			Analytical Model (Ref. [11] / [21])	% difference between analytical and Finite Element Model
	Euler-Bernoulli (2- node cubic)	Shear deformable (3-node quadratic)	% difference between Euler- Bernoulli model and Shear-deformable model		
$E_x = E_y$ (Mpa)	7.09	6.5	-9.04	7.07	0.29
E_z (Mpa)	20.63	19.28	-6.99	20.8	-0.82
$\nu_{xy} = \nu_{yx}$	0.0588	0.0757	22.28	0.0598	-1.84

$\nu_{xz} = \nu_{yz}$	0.3745	0.3694	-1.39	0.373	0.47
$\nu_{zx} = \nu_{zy}$	1.0934	1.0991	0.52	1.09	-0.31
G_{xy} (Mpa)	2.07	1.95	-6.03	2.06	0.39
$G_{yz} = G_{xz}$ (Mpa)	6.74	6.25	-7.88	6.66	1.17

Table 6: Results compared for the properties of Equisided Tetraikaidecahedron Unit cell with relative density 0.1653% with Uniform Cross-Section and Varying Cross-Section

	Uniform Cross-section	Varying Cross-Section	Ratio
Elastic Modulus (E) (Pa)	46,402	19172	2.42
Shear Modulus (G) (Pa)	14920	6183	2.41
Moment of Inertia (I) (m^4)	2.34×10^{-19}	0.965×10^{-19}	2.42
Poisson Ratio (ν)	0.4975	0.4989	1.00